Foothills structural model de-risking with 3D magnetotellurics

Federico Miorelli[1]*, Randall L. Mackie[1], Fabien Gilbert[2], Wolfgang Soyer[1]
[1]CGG
[2]TOTAL

Summary

Geophysical imaging in the foothills environment is typically hampered by complex structures, and the high cost of data acquisition in poorly accessible, rugged topography. Seismic imaging is particularly difficult due to poor signal penetration, steeply dipping structures and irregular data coverage. The use of magnetotellurics (MT) has become a successful complementary tool, due to good sensitivity to the deep resistive targets typically encountered below folded sequences of more conductive units.

Due to non-uniqueness and resolution limitations, MT 3D inversion requires additional constraints in order to recover a reliable image. These usually come from geological interpretation of available seismic and well data; however it is often the case that several competing structural models can be derived. We employ a ranking workflow that uses MT inversion to assess, via a cross-gradient operator, whether the structural models are compatible with the MT observations. We further apply 3D non-linear uncertainty estimation to address the reliability of the inversion results, obtaining a bounding envelope of the resistive anomaly.

Introduction

The geology of the Bolivian Sub-Andean Foothills comprises steep topography, thrust faulting, geology with sub-vertical dips, and generally complex compressional tectonic structures (e.g. Ballard et al, 2018). The large regional anticlinal structures hold significant gas accumulations and are active exploration targets. Obtaining good seismic reflection data continues to be problematic due to the effects of steep topography and the complex geology which degrades the signal to noise ratio and complicates accurate migration images. Strong resistivity contrasts exist between the conductive sediments and the resistive reservoir in the core of the anticlinal structures, and thus MT has been widely used to image these reservoir structures (Ravaut et al, 2002). The main drawback to using MT is its inability to resolve, from smooth blind inversions, the detailed geological structure in and around the complicated thrust structures and overturned folds. Incorporating known geological or geophysical information significantly improves inversion results, yielding more accurate and geologically reasonable results. In this abstract we build on our previous work using cross gradients against structural models to guide MT inversions and to test the validity of competing geologic scenarios (Scholl et al.,

2017). This is demonstrated with application to both synthetic and real data, and including an uncertainty analysis of the final inversion model for the synthetic example.

Geological model ranking with cross-gradients

Gallardo and Meju (2003) introduced the cross-gradient concept for the joint inversion of different geophysical data sets. The idea is to quantify structural similarity between two property distributions, rather than inter-property correlation, by looking at the norm of the cross-product of their gradients ("cross-gradient"). This norm is zero where the directions of change in the two models are aligned, or where one of the models does not change. We add the cross-gradient term as an additional regularization term to the inversion cost function

$$\Psi_{XG}(\mathbf{m}) = \beta \mathbf{m}^T \mathbf{C}_{XG}^T \mathbf{C}_{XG} \mathbf{m} \qquad (2)$$

where $\mathbf{C_{XG}}$ is the discrete representation of the volume integral of the cross gradient between two different model vectors $\mathbf{m}_1$ and $\mathbf{m}_2$ sampled on the same model grid. For a simultaneous joint inversion of two geophysical data sets, $\mathbf{m}_1$ and $\mathbf{m}_2$ are both part of the total model vector $\mathbf{m}$; i.e. $\mathbf{m}_1$ may contain resistivity values while $\mathbf{m}_2$ might contain the density values, and $\mathbf{m}$ is composed by concatenating them. The additional cross-gradient regularization term comes with its own trade-off parameter β. Using the cross-gradient as the only regularization operator does not stabilize the inverse process adequately, and so additional regularization, e.g. in form of the smoothness term, is necessary.

Instead of comparing the model gradients of two different property volumes inverted simultaneously, it is also possible to introduce *a priori* gradients derived from an auxiliary model or data set. In this case $\mathbf{m}_1$ is identical to the inverted model vector $\mathbf{m}$, while $\mathbf{m}_2$ is the auxiliary *a priori* model that remains unaltered during the inversion. Since only the direction of change matters, arbitrary numerical values can be used to create an auxiliary model resembling geological structures. Alternatively, gradients can be defined directly without setting up a model containing nominal values, so instead of creating an auxiliary model $\mathbf{m}_2$, the gradients $\nabla\mathbf{m}_2$ are used as inversion input. Auxiliary models or gradients can then be used in a sequence of inversions that try to fit the observed data while conforming to the auxiliary models (Figure 1).

Foothills model de-risking with 3D magnetollurics
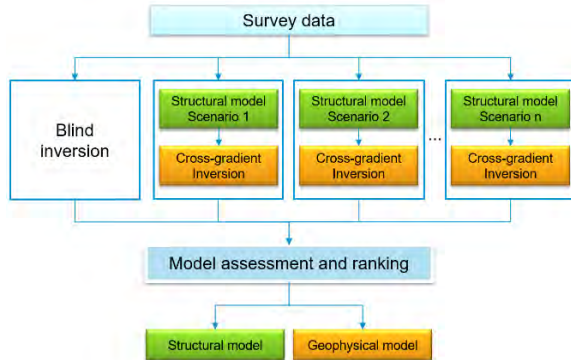

Figure 1 Workflow for cross-gradients based geological model assessment and ranking. A sequence of inversions is performed, comprising a blind (unconstrained) inversion and a cross-gradients steered inversion for each of the geological model scenarios. In the assessment phase, model interpretation together with inversion statistics are used to determine the most compatible geological model.

In this way, geological fabric can be imprinted onto the inversion result, and hypothesis testing of competing geological models can be carried out.

Synthetic example

In order to validate the proposed approach, we generated a realistic synthetic dataset, based on the geological model and topography for the area of the field data described in the next section. The survey layout consisted of 966 MT receivers on a regular grid at 800m spacing, covering an area of 36 x 16 km^2. The forward simulation mesh was made up of 8.8 million cells with 125 m horizontal cell size and 15m vertical cell size, growing with depth below topography. Full tensor magnetotelluric responses and vertical transfer functions were computed between 1000 Hz and 10000 s. The synthetic data was corrupted with Gaussian noise at a standard deviation of 2.5% of tensor row amplitude for impedances and 0.01 for vertical magnetic transfer functions.

For inversion, we employed a different mesh of 4.2 million cells, with a 200 m horizontal cell size and 25 m vertical cell size. This was done with the objective to introduce errors in discretization of topography, ultimately resulting in response distortion, which is a typical issue with datasets acquired in a rugged topography. The simulation model (Figure 2) consisted of a sequence of folded mixed clastics of variable conductivity (15 to 50 ohm-m), overlaying a target layer of 200 ohm-m. Finally, a flat crystalline basement layer of 100 ohm-m was placed at -8000 m asl. The folded overburden sequence was extracted from the geological model, while the target layer was inserted ad hoc, with the objective to assess its recovery by means of 3D inversion. Starting models for 3D inversions were
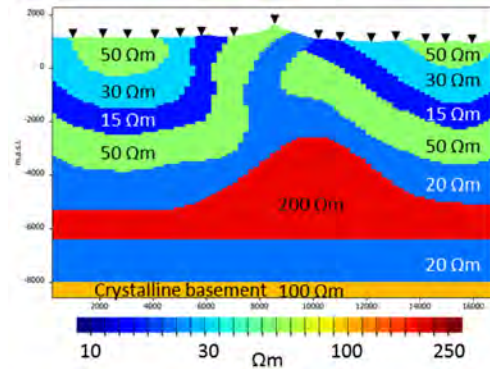

Figure 2 Slice from 3D model used in the synthetic example. The resistive target in red is a thrust-thickened sandstone at 3600-6000 m depth bgl, overlain by a folded mixed clastic sequence of variable conductivities.

uniform at 20 ohm-m and included the flat basement layer at 100 ohm-m.

To simulate uncertainty in the geological model building, and to test our ranking workflow, we generated three reference models to use for cross-gradient constraining, comprising displaced variations of the folded sequence (Figure 3). The surface dip and strike were kept at their correct values, which would be well constrained in real cases. No target horizon was added to the steering models, in order to let the inversion recover the resistor without bias. We carried out a suite of 3D inversions, comprising one unconstrained run and three cross-gradients steered inversions, one for each of the three geological model scenarios. The results for one model slice are shown in Figure 4, where colors represent the constrained runs and contours are extracted from the unconstrained inversion. All these inversions fit the data to the noise level (normalized RMS error of 1), illustrating the non-uniqueness issue in magnetotelluric inversion; the differences can be ascribed to the steering models.
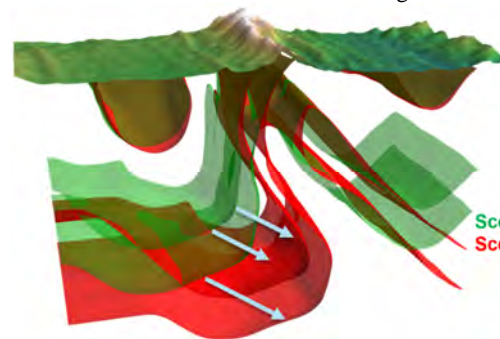

Figure 3 Simulation of geological model uncertainty used to test the model ranking workflow. Structures have been deformed in 3D with a smooth displacement field, while honoring the surface dip and strike which would be well constrained during geological model building.

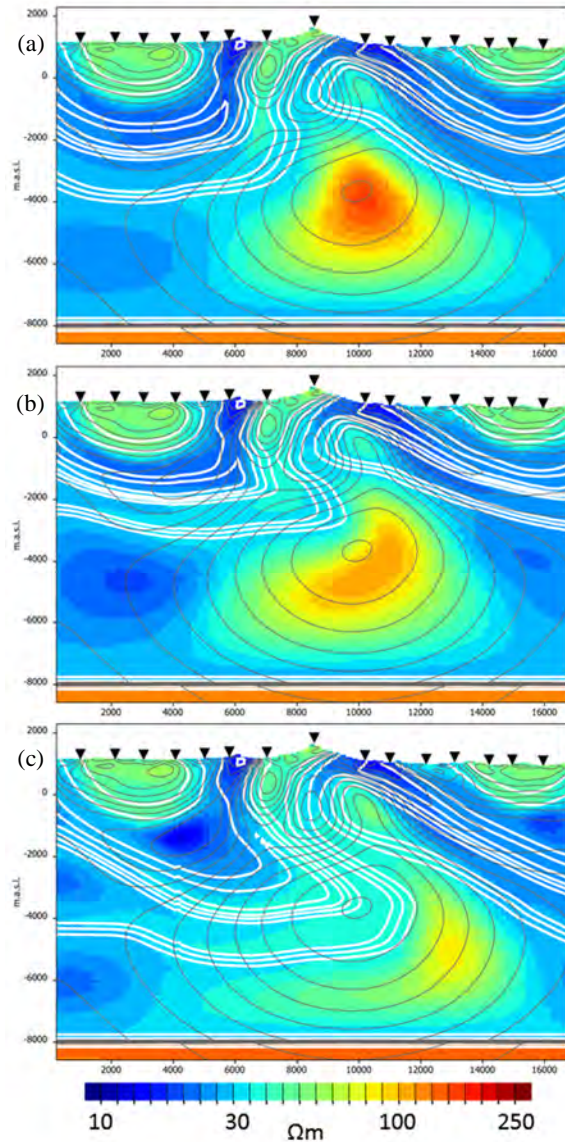**Foothills model de-risking with 3D magnetotellurics**

Figure 4 Result of model ranking workflow. Panels (a), (b) and (c) show the steered inversion in color and the unconstrained result as gray contours. Respective reference models are shown using white contours. Panel (a) corresponds to the best geological model hypothesis that would have been chosen within this suite of models.

We inspect the results looking for the model that fits the data, conforms to the structural constraints, and produces a well defined anomaly at the location of an expected thrust-thickening of the resistive formation for each scenario. Panel (a) satisfies this requirement: this geological model would have been chosen as the most compatible and is in fact corresponding to the correct geometry. Panels (b) and (c) created smeared anomalies.

Model uncertainty estimation

Geophysical inverse problems are non-unique. Through regularization and the use of *a priori* information we can derive stable and geologically reasonable inversion models. Providing an analysis of the model uncertainty is necessary for the critical task of separating inversion artifacts from robust geological features. Bayesian inference is a widely used approach but is not tractable for large three-dimensional electromagnetic problems. Another approach based on an extremal bound analysis, however, called "most squares" (Jackson, 1976; Meju and Hutton, 1992) shows great promise for quantifying model uncertainty and is computationally feasible (Mackie et al, 2018). Extremal bound analysis performed for each parameter in a large commercial sized 3D inverse model volume remains computationally challenging. However, it was shown that by carrying out extremal bound analysis on a region of interest using an appropriate 3D binary mask, then the maximum and minimum model bounds could be computed by very little additional cost beyond the original 3D inversion.
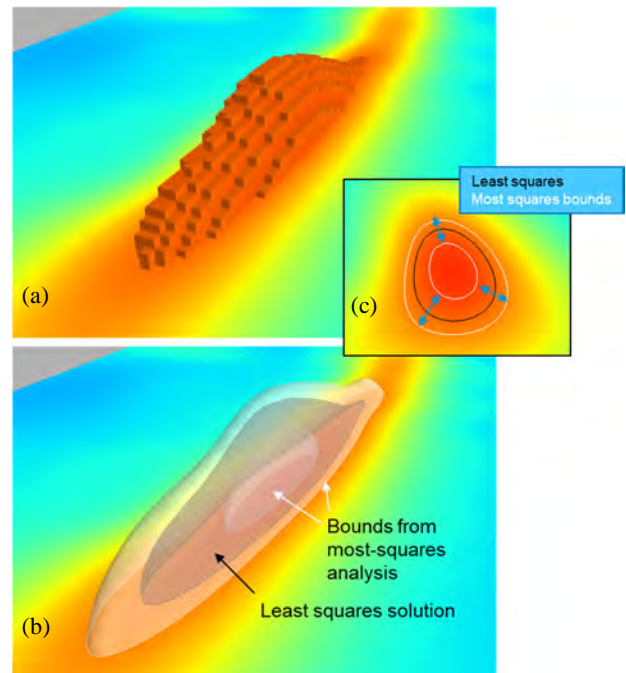

Figure 5 Result of targeted uncertainty estimation with most squares. Panel (a) shows the binary mask of voxels in the 3D model where estimation was performed, selected by means of a resistivity threshold. The iso-surfaces in panel (b) show the least squares solution (central black shell) and the extremal bounds from most-squares analysis (inner and outer white shells). Panel (c) shows a cross-section of the same iso-surfaces through the center of the anomaly.

Foothills model de-risking with 3D magnetotellurics

We applied this localized uncertainty estimation to the synthetic model described in the previous section and obtained 3D uncertainty bounds on the recovered resistor (Figure 5). Combining the geological model ranking with the uncertainty estimation, we argue we are adding significant information to the exploration problem, by not only assessing the structural model, but by also determining how reliable the target recovery is.

Application to MT data in the Bolivian foothills

TOTAL E&P Bolivie acquired MT data in the sub-Andean foothills of Bolivia over the Incahuasi field in 2013, using broadband MT systems. The objective of the survey is to image the Huamampampa formation, characterized by increased resistivity at depths of about 5-6 km bgl. The workflow applied above to the synthetic scenario has been applied to the real acquired data in a suite of inversions where we perturbed the current working geological model down to the Los Monos formation (i.e. excluding Huamampampa and deeper levels), to assess whether our methodology would be valuable in discriminating the most likely structural model. All inversions started from a two-layer model of homogenous 30 ohm-m over a 100 ohm-m basement inserted at 8km asl, and regularization (smoothing) control is for deviations from this starting model. The results are shown in Figure 6. The broad resistive anomaly from the blind inversion result under the thrusted foothills gets narrowed due to steep, lateral gradients in the geological models, and as a result the deep resistor gets vertically distributed, and its wider part pushed underneath the constrained cover where possible. The most focused result is obtained with the current geological working model A, where the anomaly is located centrally underneath the thrust zone. For scenario B the anomaly is pushed further down at the same lateral position, which is not compatible with the position where an updoming of the resistive Huamampampa formation would be expected. For scenario C the resistor is not well recovered, and is compensated by a general increase in resistivity within the post Huamampampa units. The same settings were used in all cross-gradient constrained inversions. Data fit is similar for these, with a normalized RMS of 1.4 and a slightly better fit using the current geological model as reference. Therefore the working geological model is most consistent with the MT inversion results.

Conclusions

We introduced a workflow for geological model assessment and ranking based on the use of 3D inversion with cross-gradients. The outcome of the procedure consists of a geophysical model (resistivity) as well as a validation of the geological model hypothesis which is most compatible with the observations. The value of this

approach in complex environments such as the South American foothills has been validated for a synthetic case and applied on a real exploration dataset. We further showed the application of most-squares inversion uncertainty estimation to determine the reliability of the recovered resistor. This workflow is completely generic; applied here to MT, it can be used for any kind of geophysical method involving non-linear 3D inversion (e.g. gravity, MT, seismic tomography, Soyer et al 2018).
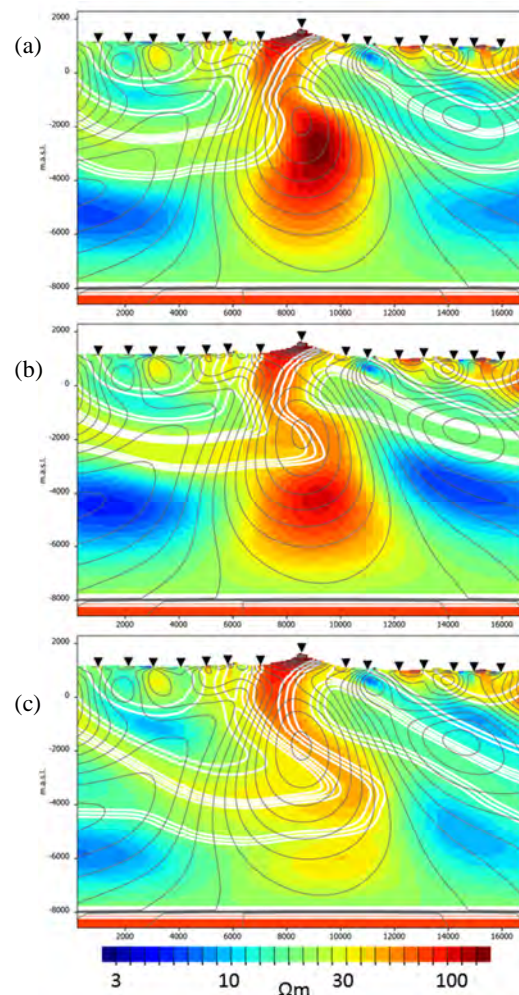
Acknowledgements

Figure 6 *Real data 3D MT inversion results (color) along a W-E line, using cross-gradients to structural reference models: (a) current geological model A, (b)/(c) scenarios B/C. Contours are blind inversion (gray) and the structural reference models (white).*

REFERENCES

Ballard, J. F., V. Spina, F. Clement, P. E. Lardin, J. M. Moron, J. M. Fleury, and P. Chaffel, 2018, An integrated approach to de-risking exploration and appraisal in structurally complex fold-and-thrust belts: Application to the Incahuasi Field (Bolivia): AAPG Memoir, **117**, 641–664, doi: https://doi.org/10.1306/13622138M1173782.

Gallardo, L. A., and M. A. Meju, 2003, Characterization of heterogeneous near surface materials by joint 2D inversion of DC resistivity and seismic data: Geophysical Research Letters, **30**, doi: https://doi.org/10.1029/2003GL017370.

Jackson, D. D., 1976, Most squares inversion: Journal of Geophysical Research, **81**, 1027–1030, doi: https://doi.org/10.1029/JB081i005p01027.

Mackie, R. L., F. Miorelli, and M. A. Meju, 2018, Practical methods for model uncertainty quantification in electromagnetic inverse problems: 88th Annual International Meeting, SEG, Expanded Abstracts, 909–913, doi: https://doi.org/10.1190/segam2018-2997269.1.

Meju, M. A., and V. R. S. Hutton, 1992, Iterative most-squares inversion: Application to magnetotelluric data: Geophysical Journal International, **108**, 758–766, doi: https://doi.org/10.1111/j.1365-246X.1992.tb03467.x.

Ravaut, P., S. Russell, P. Mallard, J. F. Ballard, D. Watts, R. Mackie, and S. Hallinan, 2002, 3D Magneto-tellurics for imaging a Devonian reservoir (Huamampampa) in the southern Sub-Andean basin of Bolivia: 72nd Annual International Meeting, SEG, Expanded Abstracts, 2417–2421, doi: https://doi.org/10.1190/1.1817205.

Scholl, C., S. Hallinan, F. Miorelli, and M. D. Watts, 2017, Geological consistency from inversions of geophysical data: 79th Annual International Conference and Exhibition, EAGE, Extended Abstracts, doi: https://doi.org/10.3997/2214-4609.201700849.

Soyer, W., R. Mackie, S. Hallinan, A. Pavesi, G. Nordquist, A. Suminar, and C. Nelson, 2018, Geologically consistent multiphysics imaging of the Darajat geothermal steam field: First Break, **36**, 67–83.